Supplementary Material

File S1. Lithology and chronology of the Rybnaya and Ulukh-Chayakh sequences.

The lithological composition at Rybnaya Mire comprises sandy clay between 400-344 cm (8.5-7.0 ka) and peat formation from 344 cm to the top (7-0 ka). At Ulukh-Chayakh Mire sandy clay accumulated between 348-310 cm and gyttja between 310 and 300 cm (>6.0 ka), followed by peat from 300 cm to the top (<6.0-0 ka). The chronology of both cores was established based on AMS radiocarbon measurements performed at Isotoptech, Debrecen, Hungary (Table S1). The ^{14}C AMS age estimates were converted to calendar years BP using the IntCal20 data set of Reimer et al. (2020) and the age-depth models were constructed using smooth spline method implemented by CLAM software (Blaauw, 2010). In the age-depth models, an age of -67 (coring year 2017 at Rybnaya) and -69 (coring year 2019 at Ulukh-Chayakh) was assigned to the surface samples of each sequence. Both sites show an inversion of some of the radiocarbon age measurements. For example, the younger age of the wood piece (4815 ^{14}C at 390 cm) embedded in the sandy clay, bottom sequence of Rybnaya, as compared to the measurements above (6727 ^{14}C at 364 cm and 4742 ^{14}C at 340 cm) suggested that this was probably dragged down from an upper layer during coring. In the age-depth models, we retained the radiocarbon measurements which produced age-depths with the lowest number of age reversals (Fig. S1). The age-depth model of the Rybnaya sequence shows a mean peat accumulation rate of 25 yr/cm (ranging 6-36 yr/cm). Ulukh-Chayakh sequence covered ~ the last 8500 years, but the chronology of the bottom part of this site (>6000 years) was based on linear extrapolation and is therefore highly uncertain (Fig. S2). The section of the sequence covering the last 6000 years had a mean temporal resolution of 21 yr/cm (ranging between 3-37 yr/cm).

Table S1. Radiocarbon dates of the Rybnaya and Ulukh-Chayakh sequences.

Lab code	**Depth (cm)**	**^{14}C age (yr BP)**	**Material dated**
Rybnaya			
DeA-20877	45	Modern (post 1950)	*Sphagnum*
DeA-23650	60	61±34	Bulk peat
DeA-20878	145	2898±30	*Sphagnum*
DeA-23651	160	3016±37	Bulk peat
DeA-23652	220	4209±41	Bulk peat
DeA-20879	245	4424±32	*Sphagnum*
DeA-20880	295	5067±37	*Sphagnum*
DeA-23653	320	5480±42	Bulk peat
DeA-20881	340	4742±45	*Sphagnum*
DeA-23654	364	6728±50	Gyttja
DeA-20882	390	4815±34	Wood
Ulukh-Chayakh			
DeA-25837	27	Modern (post-1950)	Bulk peat
DeA-23655	45	550±35	Cyperaceae seeds
DeA-25838	90	1043±23	Bulk peat

DeA-23656	135	2710±37	Cyperaceae & Rosaceae seeds
DeA-25839	144	2808±26	Bulk peat
DeA-20878	185	2331±37	Rosaceae seeds
DeA-25840	215	3447±27	Bulk peat
DeA-23658	265	4702±40	Rosaceae, Wood, leaves
DeA-25841	283	5275±34	Bulk peat
DeA-23659	311	3703±41	Organic Matter (unidentified)

Fig S1. Age depth models of the Rybnaya (a) and Ulukh-Chayakh (b) sequences

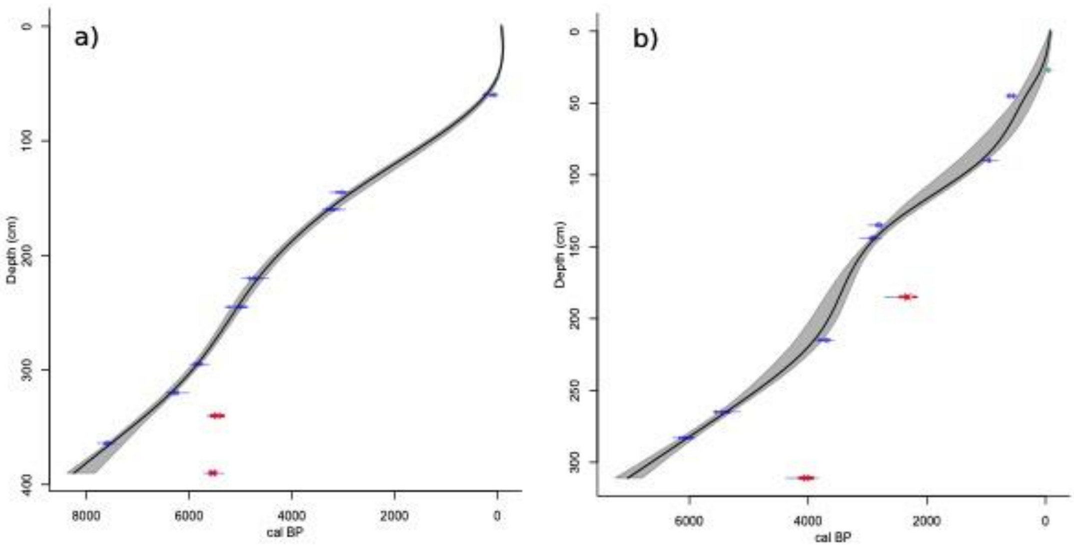

Fig S2. Deposition time of the Rybnaya (a) and Ulukh-Chayakh sequences

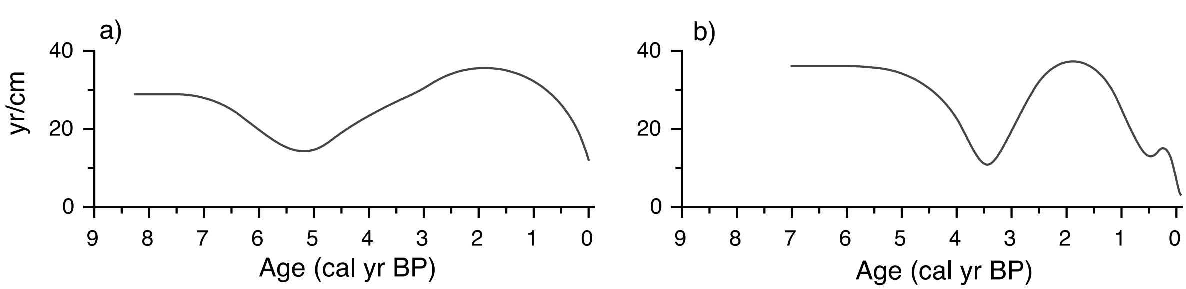

File S2. Charcoal-based reconstructions of fire history

We estimated the frequency and severity of fire episodes from charcoal peaks extracted from the macrocharcoal influx (CHAR>150 μm) using CharAnalysis software (Higuera et al., 2009). We first decomposed the total CHAR component into CHAR background (Cbackground) and CHAR-peaks (Cpeak) reflecting local fire episodes. The CHAR time series were first interpolated to constant time steps (Cinterpolated) of 30 yr for both sites. To identify the window width that maximises the signal-to-noise ratio we used a robust Lowess smoother with several window widths (e.g., 200, 300, 600, 700 and 900 yr). A Gaussian mixture model with a locally defined threshold was used to distinguish noise-related variations from local charcoal peaks. Charcoal values exceeding the 95th percentile threshold of the modelled noise distribution were identified as potential fire episodes and the fire episode frequencies were smoothed to the same window width used to determine Cbackground. We incorporated the cut-off probability for minimum count analysis to further screen and remove insignificant charcoal peaks. Evaluation of CHAR outputs including goodness of fit (GOF) and signal-to-noise index (SNI) showed that for an interpolated window width of 30 yr and a smoothing window width of 900 yr (30 yr *30 samples), the SNI was well above three at both sites (Higuera et al., 2009; 2011; Kelly et al., 2011). Therefore, we elected to use this setting for both sites (Figs. S3a, S3b). Fire frequency (FF) at each site was determined based on the total number of fires within a 900-yr time window by counting the number of charcoal peaks within that window. The charcoal peak extraction approach was designed for systems with high severity stand-replacing fires (Higuera et al., 2009), whereas fires in the study area are dominated by surface fires with an infrequent occurrence of stand-replacing fires. The high values of signal-to-noise ratio suggest that this method is suitable for charcoal peaks extractions and reliably indicates the occurrence of high-severity local fires (FigS2a,b).

Fig S2a. Peak sensitivity analysis at Rybanya (acronym SK)

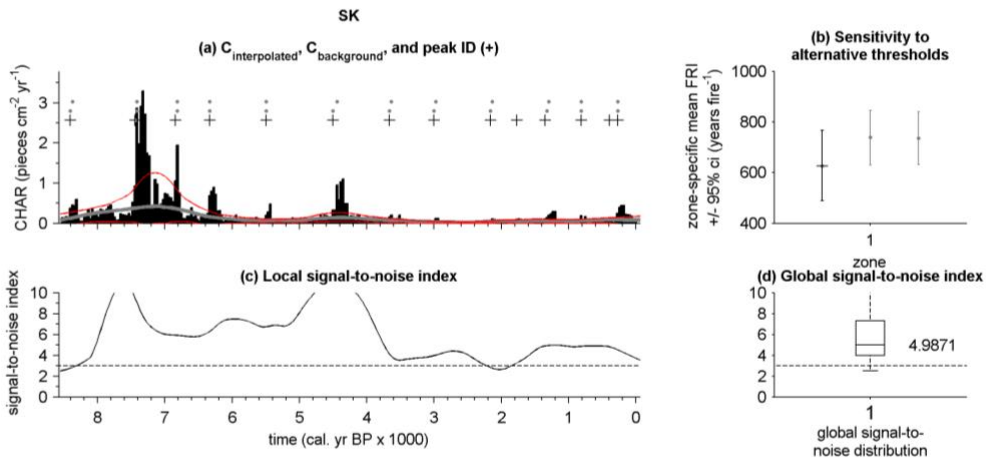

Fig S2b. Peak sensitivity analysis at Ulukh Chayakh (acronym ST).

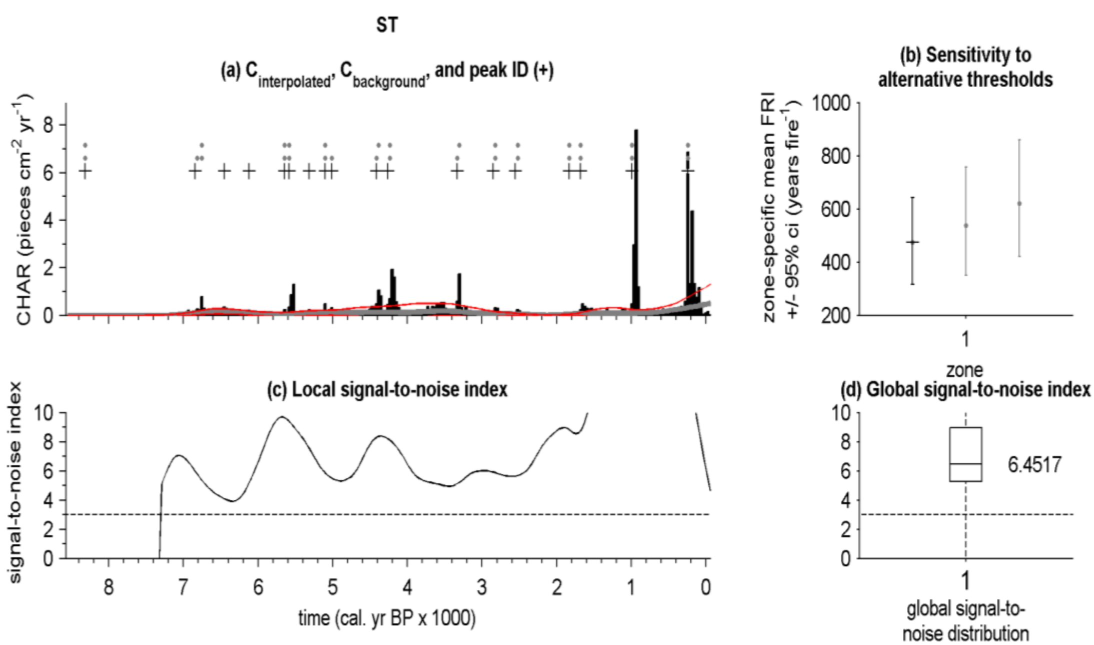

File S3a. Macrocharcoal influx (#/cm^{-2} yr^{-1}) separated into morphologies in the two sequences. Length to with ratio (*L:W*) and charcoal surface area (µm^2) were measured on selected samples a Ulukh-Chayakh sequence.

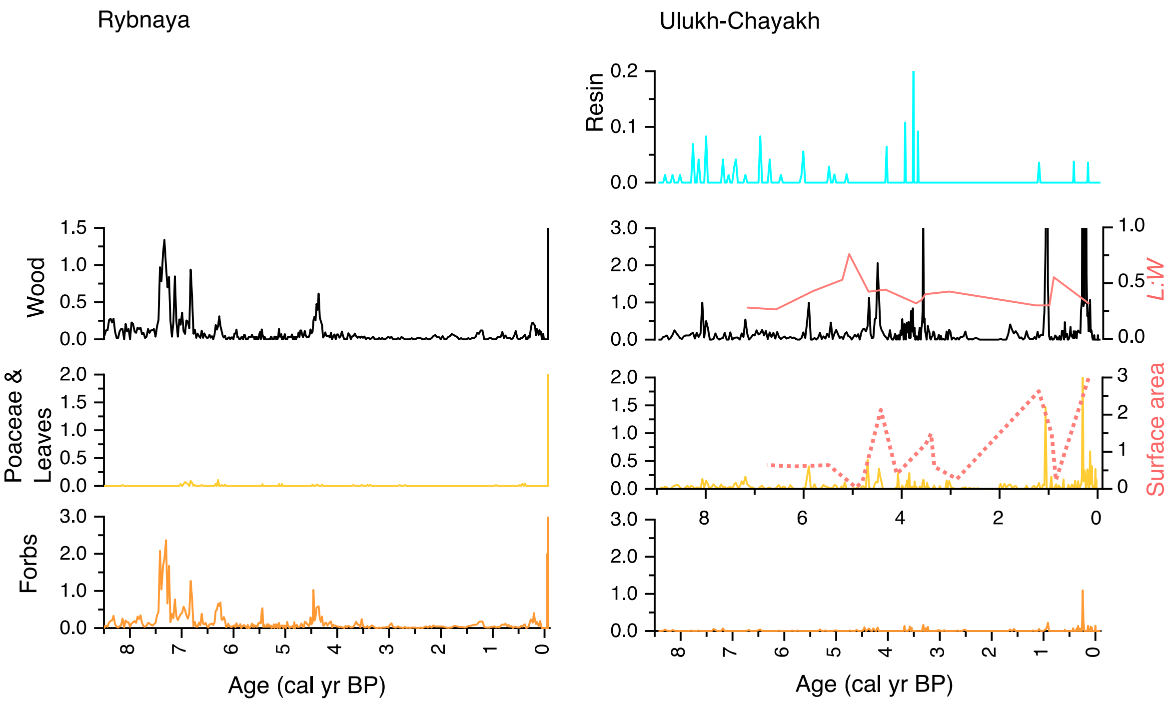

File S3b. Macrocharcoal influx (#/cm^{-2} yr^{-1}) separated into the four size classes in the Rybnaya and Ulukh-Chayakh sequences.

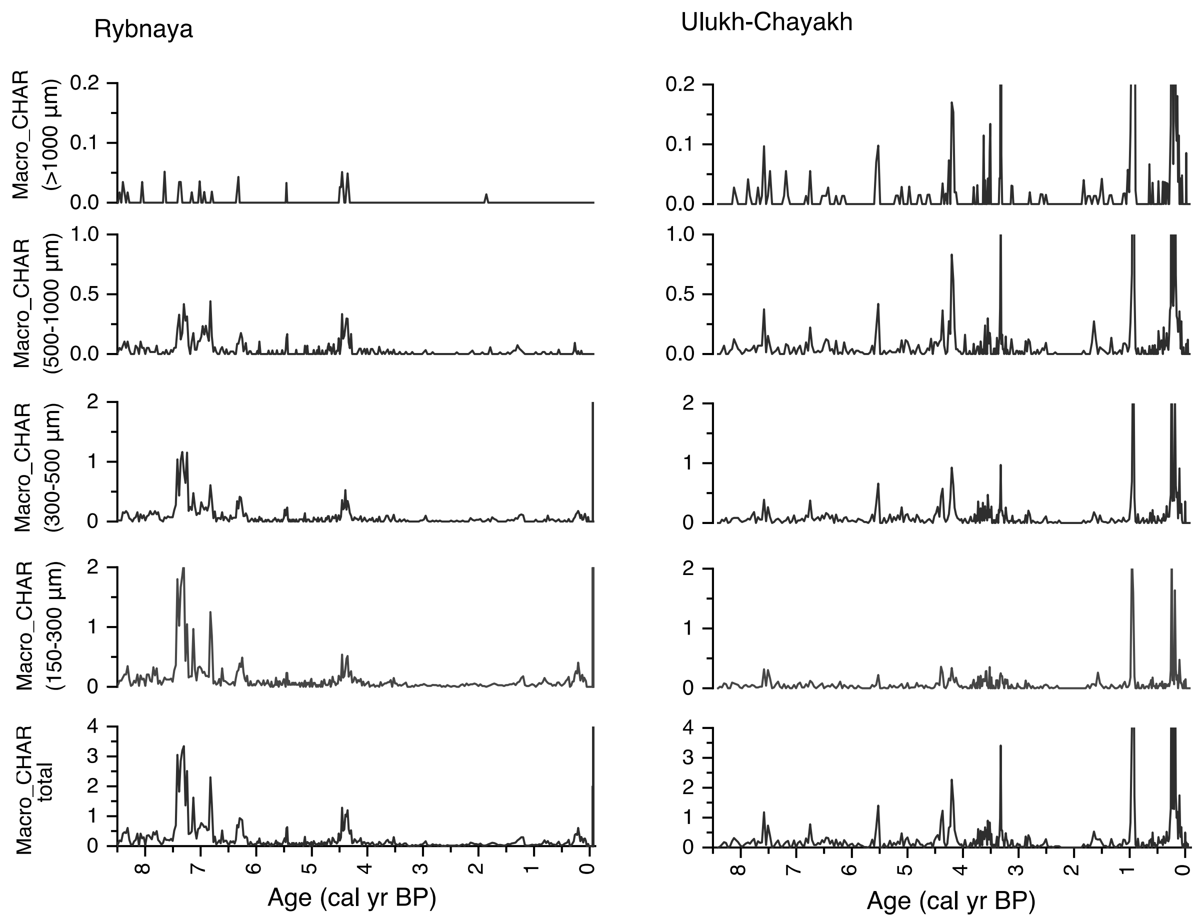

File S4a. Pollen diagram of the Rybnaya sequence.

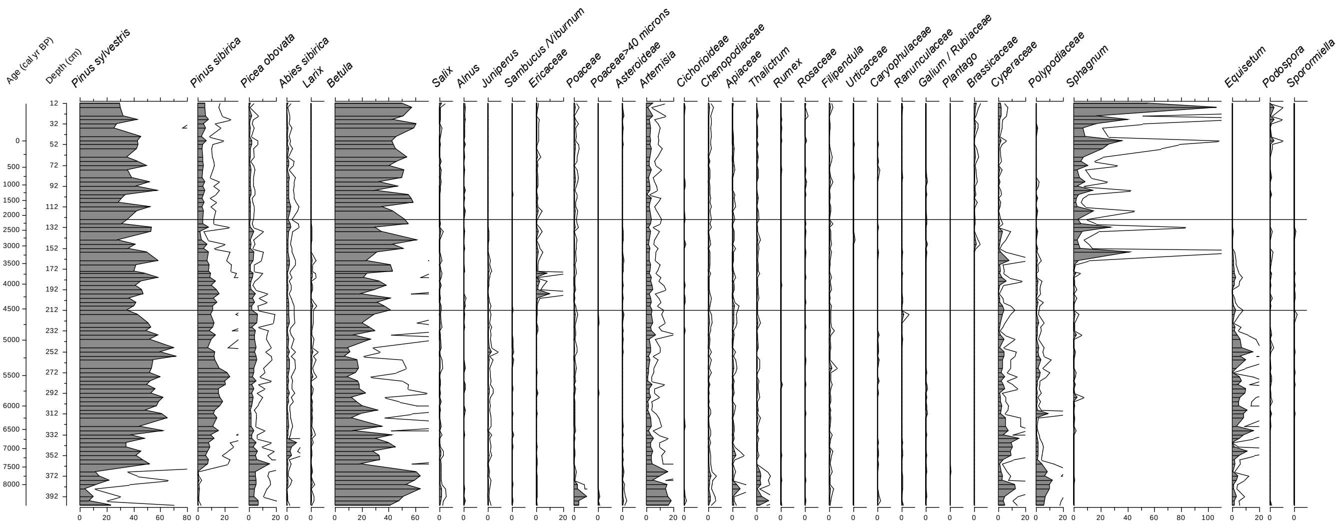

File S4a. Pollen diagram of the Ulukh-Chayakh sequence.

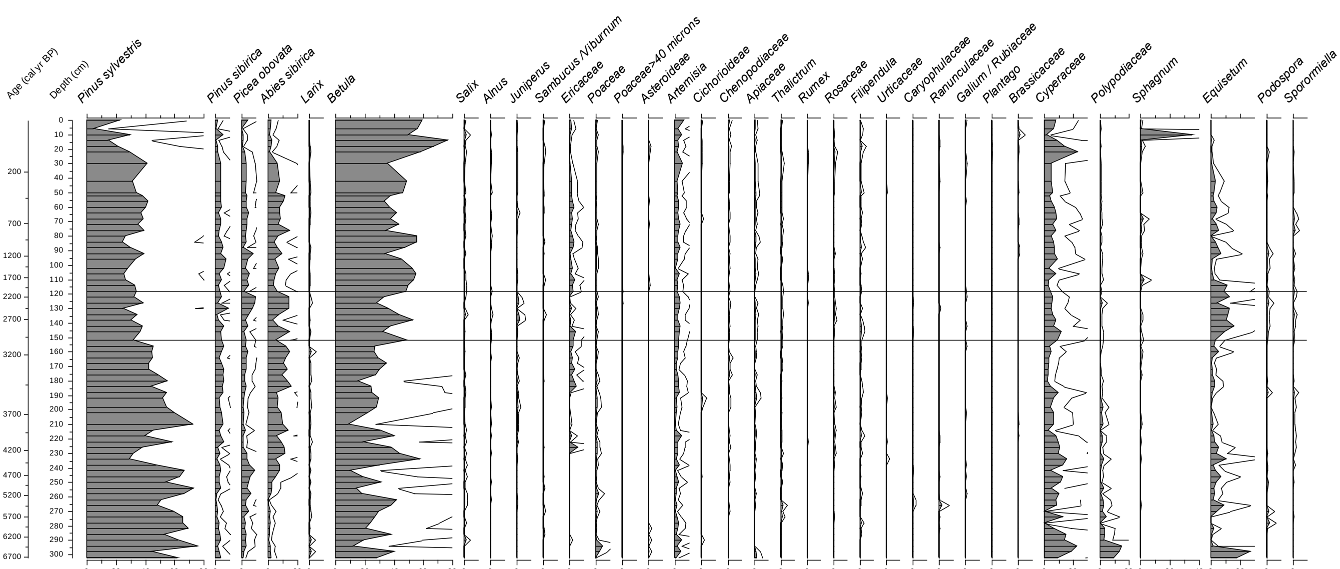

File S5. Geochemical element Ti, versus DTW (presented as Z-score) at Rybnaya (a) and Ulukh-Chayakh (b) to determine the influence of water influx (i.e., floods) on mire water table. Sedimentary Ti concentration was measured using a non-destructive Niton XL3t 900 X-Ray Fluorescence analyser (fpXRF). NCS DC73308 was employed as a Certified Reference Material (CRM). Measurement followed the procedure described by Hutchinson et al. (2016).

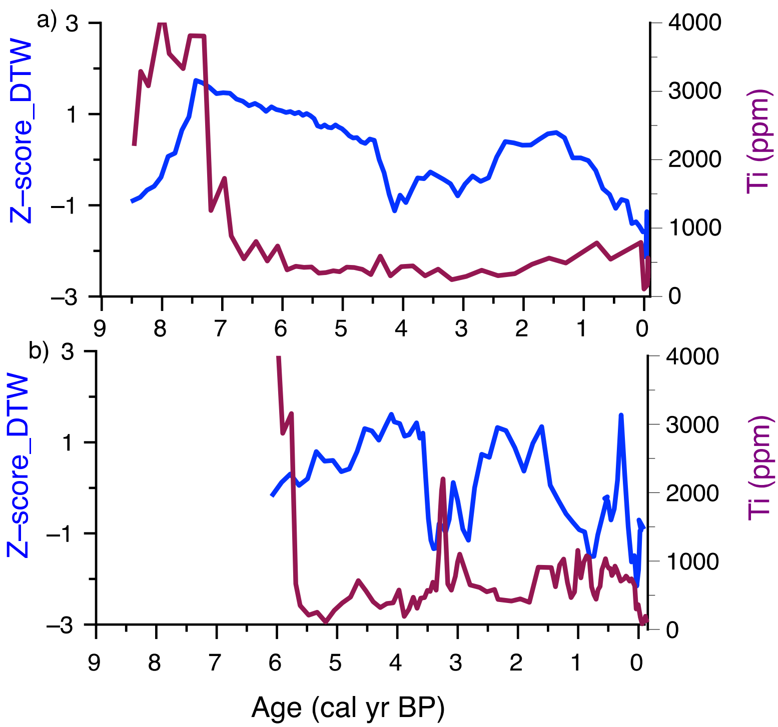

References

Blaauw, M.: Methods and code for ‘classical’ age-modelling of radiocarbon sequences. Quaternary Geochronology 5, 512–518, https://doi.org/10.1016/j.quageo.2010.01.002, 2010.

Higuera, P., Brubaker, L., Anderson, P., Hu, F., and Brown, T.: Vegetation mediated the impacts of postglacial climate change on fire regimes in the south-central Brooks Range, Alaska. Ecological Monographs 79, 201-219, https://doi.org/10.1890/07-2019.12009, 2009.

Kelly, R.F., Higuera, P.E., Barrett, C.M., Hu, F.S., 2011. A signal-to-noise index to quantify the potential for peak detection in sediment-charcoal records. Quat.Res. 75, 11e17.

Higuera, P.E., Gavin, D.G., Bartlein, P.J., Hallett, D.J., 2011. Peak detection in sediment charcoal records: impacts of alternative data analysis methods on fire history interpretations. Int. J. Wildland Fire 19, 996e10145.

Hutchinson, S.M., Akinyemi, F.O., Mîndrescu, M., Begy, R. and Feurdean, A., 2016. Recent sediment accumulation rates in contrasting lakes in the Carpathians (Romania): impacts of shifts in socio-economic regime. Regional environmental change, 16(2), pp.501-513.

Reimer, P., Austin, W., Bard, E., Bayliss, A., Blackwell, P., Bronk Ramsey, C., . . . Talamo, S.: The IntCal20 Northern Hemisphere Radiocarbon Age Calibration Curve (0–55 cal kBP). *Radiocarbon, 62*(4), 725-757. doi:10.1017/RDC.2020.41, 2020.